Heat transfer and convection onset in a compressible fluid: ^{3}He near the critical point

Andrei B. Kogan* and Horst Meyer†
Department of Physics, Duke University, Durham, North Carolina 27708-0305
(Received 23 July 2000; published 24 April 2001)

Heat transport in ^{3}He above its critical temperature T_c was studied along the critical isochore in a flat Rayleigh-Bénard cell (height $h=1$ mm, diameter $D=57$ mm). The range of the reduced temperature ϵ was $5\times10^{-4}\leqslant\epsilon\leqslant2\times10^{-1}$. The temperature difference $\Delta T(t)$ across the fluid layer as a function of the time t was measured for different values of the heat current q until steady state was reached. The crossover was observed from the regime dominated by the Rayleigh criterion for the convection onset to that controlled by the adiabatic temperature gradient (ATG), or ''Schwarzschild criterion,'' in good quantitative agreement with predictions. The slope of the convective heat current versus the reduced Rayleigh number was found to be independent of compressibility and the same as for still less compressible fluids. Plots of Nu versus Ra, both corrected for the ATG effect, are presented for early-stage convective turbulence ($1\times10^5<\mathrm{Ra}<5\times10^8$), with unexpected results for the highest values of Pr$\approx$590. The evolution of the transients $\Delta T(t)$ upon turning q on and off are described. In the nonconvective regime, the observed transient relaxation curve agrees quantitatively with predictions. In the convective regime, the shape of $\Delta T(t)$ changes qualitatively with increasing q and with ϵ. In the Appendix, new data for the thermal conductivity are presented, the impact of the ''piston effect'' on the temperature profiles inside the fluid is described, and the derivation for $\Delta T(t)$ in the diffusive regime is outlined.

DOI: 10.1103/PhysRevE.63.056310 PACS number(s): 44.25.+f, 64.70.Fx, 47.27.Te

I. INTRODUCTION

A common feature of many fluids is a very small value of their isothermal compressibility β_T. The assumption of low β_T is one of the several validity conditions of the so-called Boussinesq approximation [1], often used in hydrodynamics. The other ''ingredients'' needed for the Boussinesq approximation to apply include, for example, the requirement that the fluid properties be temperature and density -independent within the layer under consideration and are discussed in detail later in the text.

The primary focus of our paper is to study the hydrodynamic effects, which are specific to highly compressible fluids. This is achieved by designing the experimental setup and the measurement method so as to preserve the validity of all the assumptions made in the derivation of the Boussinesq equations except for the assumption of the incompressibility. Near-critical fluids are particularly convenient for studying the influence of the large β_T on the hydrodynamics because of the strong dependence of β_T on the distance from the critical point. As a result, one can investigate both the highly compressible and moderately compressible regime in the same experiment.

The second feature of near-critical fluids, which is taken advantage of in this paper, is the possibility to achieve extremely high values of the Prandtl number Pr as the critical point is approached. The flow at large Pr is usually difficult to study experimentally. This is because in simple fluids or gases, the values of $\mathrm{Pr}=\nu/D_T$ (with ν being the dynamic viscosity and D_T the thermal diffusion coefficient of the fluid) are typically of the order of 1, because the same mechanism (molecular collisions) is responsible for the dissipative flow of both heat and momentum. To exhibit a large value of Pr, a ''regular'' fluid must possess an unusually high value of ν (viscous organic oils, tar, etc.) which introduces experimental difficulties. Near the critical point however, the transport is dominated by the long-range correlation effects and as a result, $D_T\rightarrow0$, a signature of the so-called ''critical slowing down.'' Therefore very high Prandtl numbers, up to 590 in this paper, can be achieved despite the very small value of the weakly divergent viscosity of near-critical He^3 (approximately 16.7 μP). In this paper, we are interested in the effects of Pr values on the hydrodynamics, and we find unexpected results for the largest values of Pr.

We are studying a classical problem of Rayleigh-Bénard (RB) convection with particular emphasis on the region very close to the convection onset and also on the regime of beginning turbulent convection for Rayleigh numbers $\mathrm{Ra}<5\times10^8$. Existing theories [2,3] describe the onset of convection for incompressible or only moderately compressible fluids [4]. For a compressible fluid and fluid columns of large height, the ''Schwarzschild''—or ''adiabatic temperature gradient'' (ATG) criterion—replaces the usual ''Rayleigh criterion'' in determining the onset of convection. The stabilizing effect of the ATG on a large air column is well known in atmospheric sciences [1,5], but until recent experiments [6,7] the ATG effect had been ignored in laboratory experiments, where it is usually much too small to be observed. The assumption of fluid incompressibility, which is equivalent to assuming that the layer is sufficiently thin, leads to the so-called Rayleigh condition for the onset of convection [8]. According to this criterion, the mechanical stability of a horizontal layer of a pure fluid heated from below is determined by the strength of dissipative mechanisms characterized by

*Present address: Department of Physics, MIT, Cambridge, MA 02139.
†Author to whom correspondence should be addressed. Email address: hm@phy.duke.edu

the viscosity and thermal conductivity coefficients. The increase of the fluid compressibility is expected to give rise to a qualitatively different additional source of mechanical stability, described by the ATG, which does not depend on the dissipative coefficients. As a result, a compressible fluid heated from below remains stable and does not start convecting until ΔT becomes much larger than the onset value calculated from the Rayleigh condition. Our goal was to observe the crossover in the convection onset from the Rayleigh—to the ATG regime and to verify the corresponding stability calculations [9–12].

Our heat transfer experiments with a RB cell are performed in He^3 close to the critical point, as defined by the reduced temperature $\epsilon=(T-T_c)/T_c$ with $T_c\approx 3.318\,\mathrm{K}$ (NPT-90 scale). We measure the temperature difference ΔT across the fluid layer for a constant heat flow q, both in the transient $\Delta T(t)$ and the steady-state $\Delta T(\infty)$ regimes, as will be explained below. In the first part of this paper, we are interested in the regime close to the onset of convection. We are measuring the heat dependence of the temperature difference ΔT across the fluid layer at several different values of ϵ along the critical isochore $\overline{\rho}=\rho_c$. These measurements span approximately three decades in β_T. This investigation was stimulated by our recent experiments on the density equilibration of ^{3}He near T_c following a small disturbance of the cell temperature [13,14]. One of the effects observed in that work was the convective enhancement of the fluid equilibration rate. The magnitude of the temperature disturbance, necessary to observe convection, was independent of ϵ over at least the range of $5\times10^{-3}<\epsilon<5\times10^{-2}$, where such studies were performed. These observations prompted us to do an experiment, which would directly test the available predictions for the stability of a compressible fluid and, in particular, verify the Schwarzschild criterion.

In the second part, we investigate the behavior of the fluid in its convective state. In the regime close to the onset we compare the convective heat flow as a function of the Rayleigh number Ra with that obtained in other experiments. Here $\mathrm{Ra}=\alpha_P g h^3\Delta T/(\nu D_T)$, where α_P is the coefficient of thermal expansion at constant pressure, g is the gravitational acceleration, and h the fluid layer height. In the regime of early turbulent convection we present the Nusselt number Nu as a function of Ra for various Prandtl numbers Pr up to about 590, the largest number investigated so far. Here $\mathrm{Nu}=\Delta T_{\mathrm{diff}}/\Delta T$, where for a given heat current q, ΔT_{diff} is the temperature difference that would have been measured if the fluid had been in the nonconvecting state. (For a more detailed discussion of Nu we defer to Sec. IV.)

In the third part, we study the transients $\Delta T(t)$ after turning the heat current q on and off. In the nonconvective regime, the transient and corresponding relaxation times are compared with predictions. In the convective regime we describe the observed unusual temporal profiles of the transient and their evolution with changing q and ϵ.

In the Appendix, we describe the new data for the thermal conductivity of He^3 obtained during the measurements presented in this paper. We also discuss the influence of the Piston effect on the temperature dynamics in the diffusive regime and consider two different boundary conditions, one of them used in our experiments.

II. BACKGROUND

We consider a horizontal fluid layer of height h and density ρ in the gravitational field with acceleration g. The mechanical stability of a layer of a compressible fluid was first analyzed by Gitterman and Steinberg (GS) [9,10], as reviewed by Gitterman [11], and very recently by Carlès and Ugurtas (CU) [12]. In the limiting case for an uncompressible fluid the onset condition $\Delta T_{\mathrm{onset}}$ is given by the Rayleigh criterion

$$\Delta T_{\mathrm{onset}}=\mathcal{R}\times\frac{\nu D_T}{\alpha_P g h^3}, \tag{1}$$

where $\mathcal{R}$ is the critical Rayleigh number ($\sim$1708 for aspect ratio $\Gamma=\infty$), while for a very compressible fluid near the critical point, the ATG criterion dominates. The latter is derived from the requirement that the direction of the force acting on any fluid particle when it is displaced adiabatically by a small distance is opposite to the direction of the displacement. The resulting stability conditions are as follows: the fluid will remain stable when heated from below as long as the temperature gradient has no horizontal component anywhere in the fluid, and $\Delta T<\Delta T_{\mathrm{ad}}$, where

$$\Delta T_{\mathrm{ad}}=\frac{hgT\alpha_P}{C_P}=\rho g h\left(1-\frac{C_V}{C_P}\right)\left(\frac{\partial T}{\partial P}\right)_\rho. \tag{2}$$

In the two expressions above, C_P and C_V are, respectively, the heat capacity at constant pressure and volume of the fluid. We note that along the critical isochore, as $T\to T_c$, where $C_V/C_P\to 0$, the ATG inequality $ds/dz>0$ can be shown to reduce to the condition $d\rho/dz<0$. Here s is the entropy and z the vertical coordinate [See Ref. [8] Chap. 1, Eq. (4.3)]. This means that for the fluid to remain stable, the zero-gravity density gradient due to the temperature inhomogeneity associated with the heat flow, $(\partial\rho/\partial T)_P(\Delta T/h)$, cannot be larger than the density gradient due to the compression of the fluid under its own weight under isothermal condition, $(\partial\rho/\partial P)_T\rho g$, as can be seen from Eq. (2).

As mentioned before, the role of the adiabatic gradient effect in noncritical fluids is negligible in laboratory experiments; for example, in liquid ^{3}He at $T=2.6\,\mathrm{K}$, which is well below T_c, and for a layer of 1 mm thickness, we calculate $\Delta T_R=750\,\mu\mathrm{K}$, while $\Delta T_{\mathrm{ad}}=1.3\,\mu\mathrm{K}$.

In their pioneering work, Gitterman and Steinberg [9–11] developed a general expression that includes the crossover between the two limiting situations, and this was used [15] to calculate the curve for the onset of convection in ^{3}He along the critical isochore above T_c. This problem was reexamined in Ref. [12] where ''matched asymptotic descriptions'' techniques were used to derive linearized perturbation equations. With their method, which they claimed to be rigorous, CU showed that the $\Delta T_{\mathrm{onset}}$ is the sum of the terms in Eqs. (1) and (2):

$$\Delta T_{\mathrm{onset}}=\Delta T_R+\Delta T_{\mathrm{ad}}, \tag{3}$$

and they compared the numerical results over a wide range of reduced temperatures for the case of CO_2 with those obtained from the expressions of GS. They found that the differences between the two methods amounted to less then 0.2%.

Near the critical point, experiments on convection were performed by Assenheimer and Steinberg [16] who studied the convective flow pattern formation and dynamics along several isochores, including the critical one. In their experiments a room-temperature fluid, SF_6, was used over two decades in ϵ to achieve a wide range of variability for parameters characterizing Rayleigh-Bénard convection. However, because their cell was very thin, the expected $\Delta T_{ad}(T)$ was very small in comparison with ΔT_R in their range of reduced temperatures and therefore was undetectable. More recently however, Ashkenazi and Steinberg [17,7] observed the ATG for SF_6 in a RB cell of $h=10$ cm from the onset and disappearance of vertical velocity, and found agreement with predictions.

Also recently, results of an experimental study of convection in ^{4}He ($T_c=5.2$ K) over the temperature range between 3.8 and 5.9 K and a wide density range ($0.01<\rho/\rho_c<2$) were published [6,18]. This research, carried out with a cell of 20 cm height and 10 cm diameter, focused on the dynamics of highly developed turbulent states. In that work, the presence of the ATG term discussed above was observed and corrected for. This plot then evidenced scaling for all the densities up to Ra of the order of 10^{15}, and is described in detail in part II of the thesis by Chavanne [19]. More recently, measurements in ^{4}He were reported by Niemela *et al.* [20] at still higher values of Ra.

III. EXPERIMENT

A. Motivation

As mentioned before, a fluid near the critical point is a unique system which, compared to noncritical fluids, possesses unusually high β_T and Pr values. The experimental apparatus used in this paper was designed with the primary goal of studying the conditions for the convection onset in a highly compressible fluid. However, our steady-state $\Delta T(t=\infty)$ vs q data also allow to explore the heat transfer at large heat currents. This area is of interest due to the existing predictions of a universal power-law behavior of the Nusselt curve at high Rayleigh numbers, which were recently challenged by several experimental and theoretical groups [7,21,22]. Performing such measurements on critical fluids is desirable because it allows to study flows at large Prandtl numbers unattainable otherwise. However, the comparison of our data to those by other groups is limited by the fact that in our experiments, the effects due to anomalously large β_T and anomalously large Pr cannot be separated. The comparison then relies on the proposed method to ''correct'' for the compressibility-related effects by utilizing the so-called ''potential temperature'' in the analysis (Sec. IV A 1).

This problem can be solved in the future by performing measurements in several cells that have different fluid layer thickness, because the compressibility effects decrease with the layer height. Such a study would be especially interesting because of the unexpected results obtained in this work at the highest β_T and Pr combination (the data closest to T_C), however it was beyond the scope of our current program.

The heat dependence of $\Delta T(q)$ as a function of q was determined at 22 different values of ϵ, the reduced temperature of the top plate. The heat transport was studied by measuring $\Delta T(t)$ across the horizontal fluid layer for different values of q, corrected for the heat flow through the side walls of the cell. The temperature range was $5\times10^{-4}\leqslant\epsilon\leqslant2\times10^{-1}$, which corresponds to Prandtl numbers $590\geqslant \mathrm{Pr}\geqslant 2$ and to compressibilities $7\times10^{-4}\geqslant\beta_T\geqslant1\times10^{-6}$ cm^2/dyn, larger than $\beta_T\simeq2.4\times10^{-7}$ cm^2/dyn for the ideal gas at $T=3.5$ K and $\rho=\rho_c$. Short accounts of this work including both the steady-state and transient results have been reported [23–25].

Besides the questions of the mechanical stability of compressible fluids against convection and heat transport at large values of Ra, we were also interested in the transients $\Delta T(t)$ after turning q on and off. This was stimulated by the substantial current interest in developing efficient numerical algorithms for computing compressible flows. Numerical simulations starting from the complete system of hydrodynamic equations are being developed by Amiroudine and co-workers [26]. The experimentally recorded time dependence $\Delta T(t)$ provide data that can be directly compared to the results of such calculations, because the physical properties of He^3 needed for such comparisons are available over a wide range of reduced temperatures. Preliminary comparisons have been made with the experimental transient profiles in ^{3}He [27].

In the diffusive regime (without macroscopic convection) the theory for the temperature relaxation in a compressible fluid at constant average density has been developed by Onuki and Ferrell [28]. This relaxation does not follow the usual diffusion equation at constant pressure due to the existence of adiabatic energy transfer or ''Piston effect.'' The relaxation curve $\Delta T(t)$ as well as the temperature profile inside the fluid can be calculated analytically (see the Appendix). Measuring the relaxation curve in the diffusive regime allows for an independent check of the experimental setup. Also, as explained later in the text, obtaining the corresponding relaxation times τ allowed to correct the previously measured [29] values of the thermal conductivity λ and eliminate the inconsistencies [30] between the calculated and measured values of τ.

B. Apparatus and procedures

The low-temperature section of the apparatus including the RB cell is schematically shown in Fig. 1. The fluid layer is bound by two 1.5-cm-thick horizontal copper plates separated by a $\approx$0.3-mm-thick stainless steel spacing wall that is soldered onto the bottom plate without leaving any gaps. This wall, a poor heat conductor, is soft soldered to the bottom plate and extends beyond the top plate via a tight fit, leaving a small gap of 0.02 mm. An indium ring between the top plate and the spacer provided a vacuum-tight seal. The copper surfaces facing the fluid are made parallel to 0.025 mm or better. After the cell was mounted on the cryostat, it

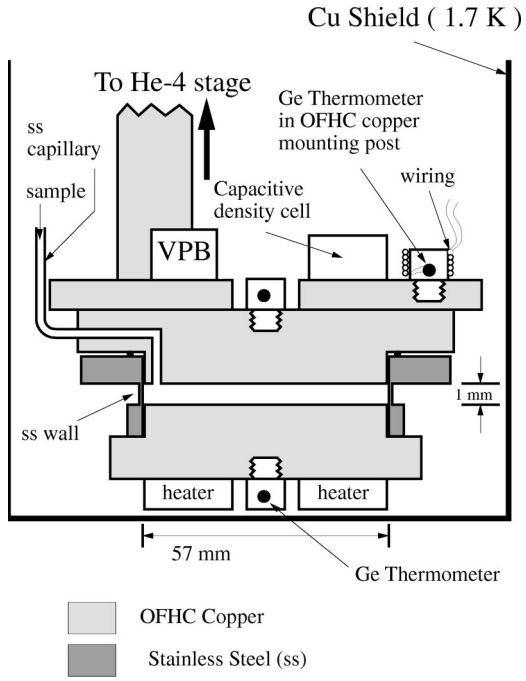

FIG. 1. Schematic presentation of the low-temperature assembly including the Rayleigh-Bénard and the density cells. All Ge thermometers are mounted and wired identically.

was leveled to ensure that these surfaces were horizontal to better than 0.5°. Two Germanium temperature sensors were mounted on the top plate of the cell, which could be interchangeably used for the temperature control and monitoring. Another sensor was mounted on the bottom of the cell to measure the temperature differences across the fluid layer. The power was supplied to the bottom plate by a commercial metal film resistor used as a heater.

The cell height h was chosen to allow measuring the predicted ΔT_{ad} from the ATG with sufficient accuracy while minimizing the diffusive fluid relaxation time, which is proportional to h^2 and diverges as $T \rightarrow T_c$. As a compromise, we chose h to be 1.06 mm, for which we calculate $\Delta T_{\mathrm{ad}} \approx 3.6\,\mu$K and relaxation times of the order of 10^3 s and 10 s at $\epsilon = 10^{-3}$ and 10^{-1}, respectively. Another advantage of this choice for h was that it permitted reaching both the asymptotic ''Rayleigh'' and ''ATG'' regimes as well as investigating the crossover region between them [31]. The cell was filled with ^{3}He via a 0.1-mm inner diameter stainless-steel capillary to a density within 0.5% of ρ_c by monitoring the capacitive density cell connected in parallel, and then sealed off from the sample handling system. The amount of sample within the capillary was estimated to be less than 0.5% of the fluid mass in the RB cell.

The germanium resistor thermometry using ac bridge systems had a temperature resolution of 0.3 μK. These bridges enabled controlling the temperature of the upper plate and measuring ΔT. We used commercial metal film resistors as low-temperature standards in all three bridges and found that they performed as good as the traditionally used wire-wound resistors. The typical time constant of the phase-sensitive detectors was either 0.3 or 1.25 for different measurements.

The density of the fluid was determined via its dielectric constant in a separate cell, thermally anchored to the temperature-controlled platform, to which the top of the RB cell was attached (see Fig. 1). A capillary (not shown) from the density cell and valves at room temperature enabled fluid exchange with a gas handling system and the RB cell. The ratio-transformer bridge system was of the same type as in previous experiments [29] and permitted a density resolution of $\delta\rho/\rho_c = 1 \times 10^{-6}$ near ρ_c. The techniques for density and temperature calibration and measurements used in this paper are analogous to those in previous thermal conductivity and shear viscosity experiments [29,32,33].

The critical temperature T_c was located by determining the compressibility β_T at ρ_c from density measurements along an isotherm at the temperature T known from the *T-90* scale. By identifying β_T with the data by Pittman *et al.* [34], the value of ϵ of this isotherm was determined, and therefore T_c. The uncertainty was estimated to be $\delta\epsilon = \pm 1 \times 10^{-4}$. The absolute value was found to be $T_c = 3.3189(10)$ K, consistent with $T_c = 3.3190(10)$ in other experiments described in Ref. [14], but slightly higher than $T_c = 3.3169(10)$ K from experiments of Ref. [34] after the correction, 6.9 mK, from the T_{58} to the T_{90} ^{4}He scale.

During the experiments, the temperature of the top plate was controlled at a fixed value with a short-term stability of $\pm 0.8\,\mu$K for most experiments and with slow drifts typically within 3–5 μK over tens of hours. In a measurement, the power was applied to the bottom plate and a change in the temperature difference across the fluid $\Delta T(t)$ was measured as a function of time and its steady-state value recorded. To improve the resolution, we averaged the results of 5–40 measurements for each heat, depending on the magnitude of ΔT, to reduce the scatter due to the equipment noise to ± 0.3 μK. Because of the time limitations, lengths of individual traces did not exceed about 1800 s taken at $\epsilon = 2 \times 10^{-3}$. All the results were obtained over a period of 8 months continuous data recording.

We calculate the heat flux q through the fluid layer by subtracting the fraction of the heat that travels through the side wall from the total power applied to the bottom plate. The thermal resistance of the sidewall was measured before introducing the sample into the cell. The sidewall is treated as a heat conductor parallel to the fluid layer and it is assumed that no heat is exchanged between the fluid and the sidewall. Without convection in the cell, this was demonstrated to be a very good approximation in a recent numerical simulation of thermal transport experiments in similar experimental geometries in normal He^4 by Murphy [35], both for steady-state transport and for time-dependent diffusive transport at low frequencies. The presence of convection in the cell in general is expected to make this assumption weaker, in particular in highly turbulent states characterized by a nonlinear temperature profile across the fluid layer [36].

Because the top plate temperature is kept constant during the heat flow, the average fluid temperature increases with q. The values of Ra, Nu, and Pr have been calculated for average values of ϵ, and care was taken to ensure that the changes in parameters for a given ϵ of the top plate were

only of the order of a few percent for the highest values of q used.

Finally we briefly consider the thermal boundary resistance R_b at the interface between the parallel copper plates and the fluid. It is difficult to measure R_b in a ''normal'' fluid as opposed to superfluid ^{4}He where many measurements have been reported (for a review see Ref. [37]). The measurements in the normal phase of liquid ^{4}He by an ac method [38] give a much larger value well above the superfluid transition than do more conventional dc measurements by Lipa and Li [39], and have been questioned in Ref. [35]. Based on the results of Ref. [39], we estimate that the R_b for ^{3}He under our experimental conditions will be negligible in comparison with the thermal resistance h/λ of the bulk fluid. A divergence of R_b near T_c for fluids is expected [40], but no specific predictions have been made.

In our data analysis, we assumed the R_b to be zero. This is certainly a good assumption in the diffusive regime and is supported, for example, by the agreement between the steady-state conductivity and the relaxation-time measurements (see Sec. IV B 1). It is conceivable that the correction due to R_b could become significant at large enough Nu numbers. This subject can only be addressed after R_b in He^3 has been studied separately, in particular close to T_c.

IV. RESULTS

In this section we first present the steady-state data of $\Delta T(\infty)$ versus q and their discussion, namely, for the heat flow in the diffusive regime and just above the convection onset. Second, we present convective heat current data up to the highest Rayleigh numbers we have used and where the density variation across the fluid layer is calculated to be less than $\approx$5%. The conditions in our experiment with compressible ^{3}He are such that the first three Boussinesq criteria A, B, and C, described in Tritton's book [1] [Eqs. (14.78)–(14.80)] are satisfied. These are, respectively, (1) the relative density change $\delta\rho/\rho_c$ across the fluid layer due to the temperature change ΔT is very small (in practice less than a few percent in our experiment), (2) the density stratification due to the earth's gravity is also small (at most $\approx$4% in our arrangement, namely, at $\epsilon = 5\times10^{-4}$), and (3) $\Delta T_{ad}/T \ll 1$, which is certainly satisfied.

The last remaining condition of the validity of the Boussinesq approximation, $\Delta T_{ad} \ll \Delta T$ (see the following section) is obviously not satisfied in our experiment, and therefore the flow that we observe is not a Boussinesq flow. This leads to the change in the stability condition, which we address first. Second, we describe the ''correction'' for the adiabatic effects via the so-called ''potential temperature'' θ. The use of this correction allows to establish a correspondence between the measurements of the Nu(Ra) curve in a fluid with a nonzero ΔT_{ad} and the predictions for a Boussinesq fluid. We will show that based on the proposed correction, measurements done relatively close to the convection onset in a compressible fluid effectively probe the Nusselt curve of a truly Boussinesq fluid obtained at much larger values of Ra. This will permit a comparison of the data with those of much less compressible fluids and also with predictions.

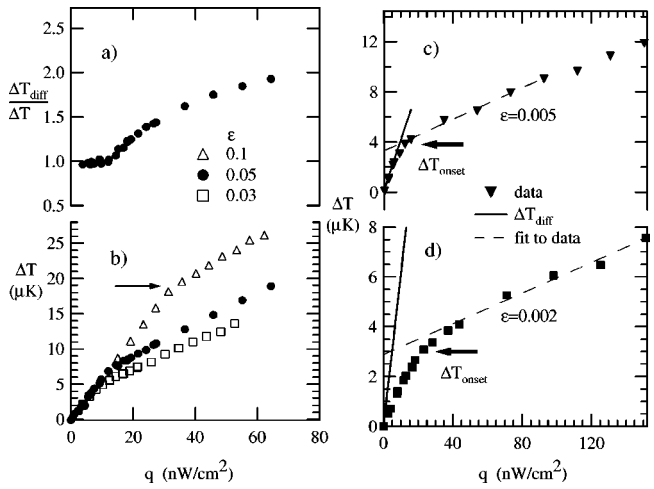

FIG. 2. (a) The Nusselt number, $\Delta T_{diff}/\Delta T(t=\infty)$, as a function of heat flux q for $\epsilon = 0.05$, showing the sharp onset of convection. (b) The onset signature (change in the slope) in the $\Delta T(t=\infty)$ vs q curves, as shown by the horizontal arrow on the top curve. (c) and (d) Similar plots close to the critical point where the onset signature becomes increasingly more rounded as ϵ is decreased.

Finally, we deal with the transient fluid response after the heat flow is turned on and off, as measured by $\Delta T(t)$, analyze the data in the diffusive regime, and present the evolution in the convective regime.

A. Steady-state data

1. Convection onset

In a nonconvecting layer, we expect the measured $\Delta T(q)$ to represent diffusive heat transport and to be given by $\Delta T_{diff}(q) = qh/\lambda$, where λ is the thermal conductivity of the fluid. When the fluid is driven into convection, the slope $\partial\Delta T/\partial q$ suddenly decreases with increasing q.

Figure 2(a) shows a plot of $\Delta T_{diff}/\Delta T$ versus q for $\epsilon = 0.05$ with a sharp break in the slope, the signature of the onset. ΔT_{diff} was calculated from the values of λ obtained in experiments described in the Appendix. Three representative plots of ΔT versus q, showing a sharp kink, are displayed in Fig. 2(b), where the arrow indicates the onset of convection. As T_c is approached further, the transition becomes less sharp, and the rounding prevents its unambiguous determination for $\epsilon < 5\times10^{-3}$. This is shown in Figs. 2(c) and 2(d) for $\epsilon = 0.005$ and 0.002, and it suggests that with diverging compressibility, the mechanical stability of the fluid might possibly be getting more sensitive to the temperature control quality, and possibly to a small tilt, if any, of the RB cell from the horizontal. It then appears reasonable to determine ΔT_{onset} as a crossing point of a linear extrapolation of the $\Delta T(q)$ curve from above the onset (dotted straight line) and the $\Delta T_{diff}(q)$ line (dashed straight line), which is based on the amended conductivity data of Ref. [29] (see the Appendix). We performed this analysis and compared the results with theory as shown in Fig. 3. Here the solid line is obtained from the expressions for the ΔT_{onset} derived in Refs.

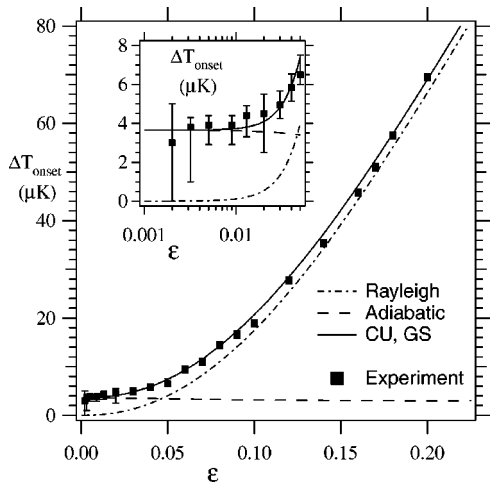

FIG. 3. Comparison of the experimentally determined $\Delta T_{\rm onset}$ versus ϵ (symbols) with theory (lines). Main figure: linear plot. Inset: semilogarithmic plot in the region where the ATG is dominant. The ''error bars'' represent the approximate width of the transition, resulting from the rounding of the onset feature, which increases as T_C is approached [see Figs. 2(c) and 2(d) and the text for explanations].

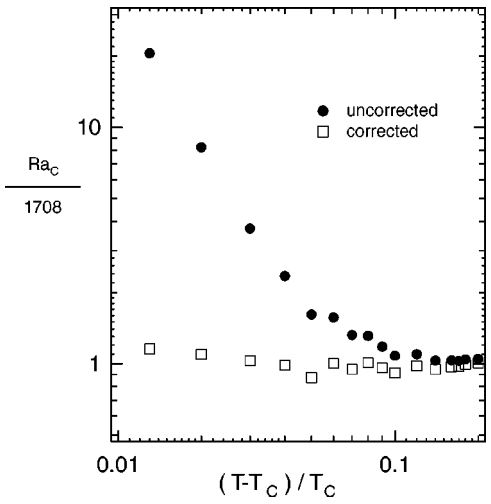

FIG. 4. The ratio $\mathrm{Ra}_c/1708$ versus ϵ where $\mathrm{Ra}_c/1708$ is given by Eq. (1) and where the corrected number $(\mathrm{Ra}_c)_{\rm corr}$ is obtained as explained in the text. The ratio $(\mathrm{Ra}_c)_{\rm corr}/1708$ agrees with the expected value of unity.

[9–11] and where static and transport properties of ^{3}He obtained in this laboratory were used (Refs. [34], [29], [32] and references therein to earlier work). Within computational accuracy, the same solid line is also obtained from Eqs. (1)–(3) as per the recent analysis of Ref. [12]. For comparison, we also show curves representing the individual $\Delta T_R(\epsilon)$ and $\Delta T_{\rm ad}(\epsilon)$ from Eqs. (1) and (2). The agreement is very good, and this represents the first systematic study of the convection onset crossover into the regime where the ATG dominates.

In this and the next section, we will often be making use of the so-called ''potential temperature'' θ defined as $\theta = T - T_{\rm ad}$, T being the temperature of the fluid. $T_{\rm ad}$ is an arbitrary solution of the equation

$$\frac{\partial T}{\partial x} = -\frac{\Delta T_{\rm ad}}{h}, \tag{4}$$

where $\Delta T_{\rm ad}$ is defined by Eq. (2). Thus θ is defined to within an arbitrary constant, however, as will be seen below, only the change $\Delta\theta$ across the fluid will be needed.

The potential temperature θ is useful because of the following property, discussed in Ref. [1] [Eqs. (14.112) and further equations]. Suppose the fluid under consideration satisfies the criteria of the Boussinesq approximation, described above, except the requirement

$$D \equiv g\alpha_P h T/C_P \Delta T \ll 1$$

or equivalently

$$\Delta T_{\rm ad} \ll \Delta T \tag{5}$$

(notations as in Ref. [1]). This is precisely the case for the experiments described in this paper. It can be shown [1], that under such conditions, the Boussinesq form of the equations describing the fluid can be restored if the real temperature T is replaced with the potential temperature θ. This point serves as the basis for ''correcting'' the various quantities in a high compressibility regime, when $\Delta T \sim \Delta T_{\rm ad}$, as described in Sec. IV A 2.

To demonstrate the use of θ we present the onset data in terms of the corresponding critical Raleigh number Ra_c at the convection onset, $\Delta T_{\rm onset}$, as a function of the reduced temperature ϵ. Note that the property of θ stated above immediately yields the prediction of CU as given by the Eq. (3): If true, one expects the ''corrected'' Raleigh number $\mathrm{Ra}_{\rm corr}$:

$$\mathrm{Ra}_{\rm corr} = \frac{\alpha_P g h^3}{\nu D_T} \times [\Delta T - \Delta T_{\rm ad}] \tag{6}$$

to take the value $\mathcal{R} = 1708$ at the onset, regardless of compressibility. This implies that $\Delta T_{\rm onset} - \Delta T_{\rm ad} = \Delta T_R$, which is precisely Eq. (3).

Figure 4 shows the values at the convection onset of the ''raw,'' or uncorrected, Rayleigh number Ra_c (solid circles) and the ''corrected'' Rayleigh number $\mathrm{Ra}^c_{\rm corr}$ (open squares). The ''corrected'' data in Fig. 4, divided by 1708, show the expected value of unity independent of ϵ, with less than $\pm 15\%$ error. The increasing scatter and uncertainty with decreasing ϵ reflects the subtraction in Eq. (4) of the two terms that become comparable as the ATG term in Eq. (3) dominates. For this reason, the data for $\epsilon < 0.03$ are not shown here.

2. Heat current just above the convection onset

Our second purpose was to study the initial convective state and determine the convection current $j^{\rm conv}$, which is the ratio of the convective portion of the heat current to that conducted through the fluid at the transition. This definition leads to the relation [3]

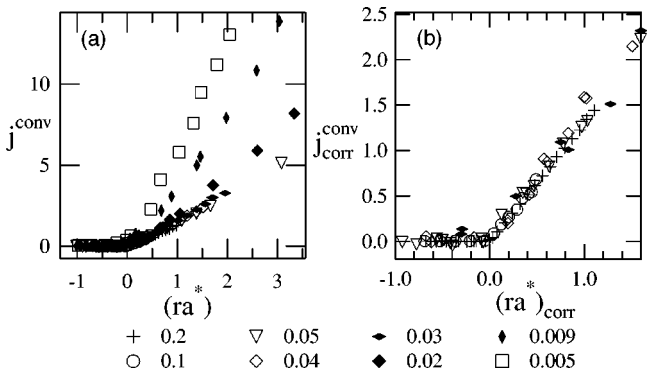

FIG. 5. The convection current j^{conv} versus the reduced Rayleigh number ra*. (a) Obtained directly from the measured $\Delta T(q)$ curves, such as shown Fig. 1. (b) Data restricted to those near the onset for $ra^*_{corr}<1$, corrected to take into account the presence of the ATG, as explained in the text. Note the difference in both the vertical and horizontal axes scales.

$$j^{conv} \equiv (Nu-1)(ra^*+1) \tag{7}$$

versus the reduced Rayleigh number $ra^* \equiv (Ra-Ra_c^{obs})/Ra_c^{obs}$ and where

$$Nu \equiv \Delta T_{diff}/\Delta T_{obs} \tag{8}$$

is the Nusselt number, with ΔT_{obs} the observed temperature change across the fluid layer. For $ra^*<0$, $\Delta T_{obs}=\Delta T_{diff}$. It was of particular interest to check whether the initial slope $dj^{conv}/d(ra^*)$ of the data in the convective state is independent of compressibility, and how it compares with results of other fluids in cells with a similar aspect ratio.

In Fig. 5(a), a plot of j^{conv} versus ra* is presented for various reduced temperatures, where again ϵ is the temperature of the top plate. For $\epsilon<1\times10^{-2}$ the rounding of the transition to the convective state did not allow us to determine the slope near $ra^*=0$. Chavanne [19] has used the concept of the potential temperature difference $\Delta\theta$ mentioned above to propose relations that correct both Nu and Ra for the effect from the ATG. Then, instead of Eq. (6) one obtains

$$Nu_{corr} = \frac{\Delta T_{diff}-\Delta T_{ad}}{\Delta T_{obs}-\Delta T_{ad}}. \tag{9}$$

Substituting the ajusted parameters Ra_{corr} and Nu_{corr} into Eqs. (5) and (6) we obtain the corrected heat current and reduced Rayleigh numbers where the relations take the following simple form:

$$j^{conv}_{corr}=[1+C(\epsilon)]j^{conv} \quad \text{and} \quad ra^*_{corr}=[1+C(\epsilon)]ra^*. \tag{10}$$

The factor $C(\epsilon)=(Ra/1708)(\Delta T_{ad}/\Delta T)$, where Ra is the uncorrected Rayleigh number, expresses the relative strength of adiabatic effects compared to dissipative forces and diverges as $T\to T_c$. The result is that both j^{conv} and ra* are rapidly ''stretched out'' by the corrective transformation as T_c is approached.

The transformed data of Fig. 5(a) are shown in Fig. 5(b) for $ra^*_{corr}<1.6$ that emphasizes the initial slope S in the convecting state. The large scatter for $\epsilon=0.04$ and 0.03 is due to the transformation from ΔT to $\Delta\theta$, but is random about the average shown by the straight line. The slope S remains unchanged for $0.03\leqslant\epsilon\leqslant0.2$ with $S=1.3\pm0.1$, as an examination of individual plots for a given value of ϵ shows. This corresponds to a compressibility range between 1.9×10^{-5} and 1.2×10^{-6} cm^2/dyn and is to be compared with $S=1.23$, 1.25, and 1.20 for liquid ^{3}He between 2.1 and 2.6 K (where S was obtained from the data in Fig. 2 of [41]), liquid ^{4}He at 2.4 K [42] and distilled water at 30 °C [43] in RB cells with similar aspect ratios. Also for comparison, the compressibilities for these fluids are 1.3×10^{-7}, 2×10^{-8}, and 4×10^{-11} cm^2/dyn, respectively, while their Pr numbers are 0.8, 0.5, and 6.0 [41–43].

It is known that the initial slope of $j^{conv}(ra^*)$ is strongly dependent on the flow pattern formed at the convection onset. The experiment with water was the only one provided with a shadowgraph optical arrangement that clearly showed the pattern to be one of concentric rolls (See Fig. 2 of Ref. [43].) We note that shadowgraph experiments on liquid ^{4}He by Woodcraft *et al.* [44] also indicate that at the onset of convection, concentric rolls are obtained in their cell configuration. For such a pattern with zero-velocity amplitude at the center, the predicted slope is 0.86 [3], while for straight rolls it is 1.42 [2]. The experimental slopes agree best with the straight roll prediction, and we note that nonconcentric, almost straight parallel rolls, have been observed by Croquette [45] with a cylindrical container when the Rayleigh number is increased very slowly. In spite of the uncertainty about the form of the convection pattern, it is noteworthy that the slopes for the fluids we have mentioned are all consistent with one another, regardless of the compressibility that varies over a factor of $\sim10^5$ between water and ^{3}He near T_c. (The effect from the different Prandtl numbers in these fluids on the predicted slope [2,3] is calculated to be insignificant.)

The data of $j^{conv}_{corr}(ra^*_{corr})$ for various values of ϵ are found to collapse onto a single line in a logarithmic plot for ra^*_{corr} numbers up to 10^4. This is shown in Fig. 6, where the data points departing from the common curve (see in particlar the two solid triangles) simply reflect the uncertainty of ΔT_{onset} for low values of ϵ due to rounding of the transition. This serves as an experimental ''proof'' of the property of the potential temperature θ stated in Sec. IV A 1. For comparison, we also show the line representing the data on ^{4}He gas at various densities [19,18], carried out in a cell of 10 cm height and 5 cm diameter, extend to much higher ra^*_{corr} numbers well into the turbulent regime.

3. Early stages of convective turbulence

Several series of measurements of ΔT versus q were carried out over a large range of q, but where the heat flow was limited so as to satisfy the Boussinesq conditions. This restriction becomes more severe as T_c is approached. For $\epsilon=5\times10^{-4}$, or $(T-T_c)=1.7$ mK, measurements were therefore taken for $\Delta T\leqslant70\,\mu$K, or $\approx0.03(T-T_c)$. As mentioned

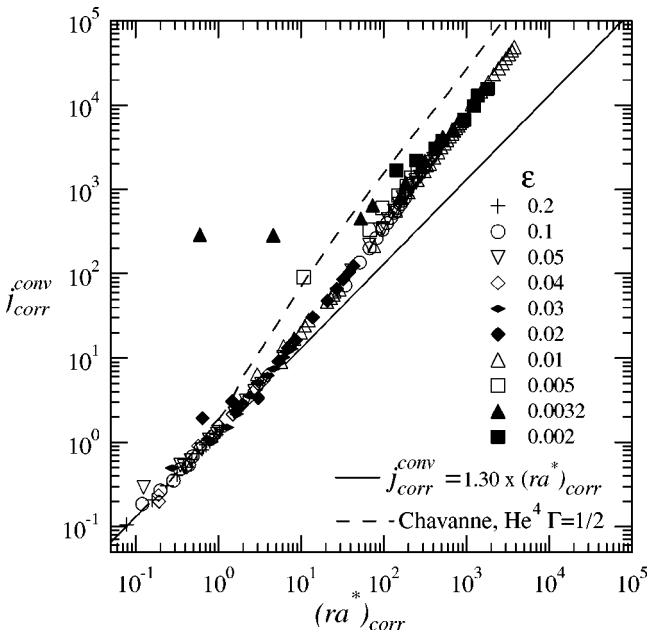

FIG. 6. The convection current $j_{\rm corr}^{\rm conv}$ versus $({\rm ra}^*)_{\rm corr}$ (symbols) in the convective regime. Also shown are the data for ^{4}He (dashed line) at various densities for the cell with $\Gamma = 1/2$, used by Chavanne *et al.*

before, the temperature of the top plate was kept constant, and hence the average fluid temperature increased with the heat current. This led to an increase of $\mathrm{Ra_{corr}}$ and to a decrease of Nu and Pr up to a few percent for $\Delta T = 70\,\mu$K. These corrections have been implemented in the calculations for all three parameters. In Fig. 7(a) we show a logarithmic $\mathrm{Nu_{corr}}$ versus $\mathrm{Ra_{corr}}$ plot for $\mathrm{Ra_{corr}} < 10^7$. For this range of $\mathrm{Ra_{corr}}$, our experiments can be compared with the very recent ones by Xu *et al.* [21] These authors worked with RB cells using acetone with Pr=4.0. The measurements by Chavanne *et al.* [19,18] at comparable values of Pr as well as those by Ashkenazi and Steinberg [7] were done at substantially higher values of Ra than ours.

There has been strong interest in convective turbulence and the most recent summary of both theoretical and experimental work has been given by Grossmann and Lohse (GL) [22]. These authors have presented a systematic theory for the scaling of Nu and the Reynolds number in strong RB convection and have identified various zones that are characterized by the relative importance of certain contributions from boundaries or bulk in the dissipation during the heat transport. In their Fig. 2 they present the phase diagram of these zones in the Ra-Pr plane. The high-precision measurements of Xu *et al.* with Ra between 10^8 and 10^{10} could be fitted by the predictions of Grossmann and Lohse (GL).

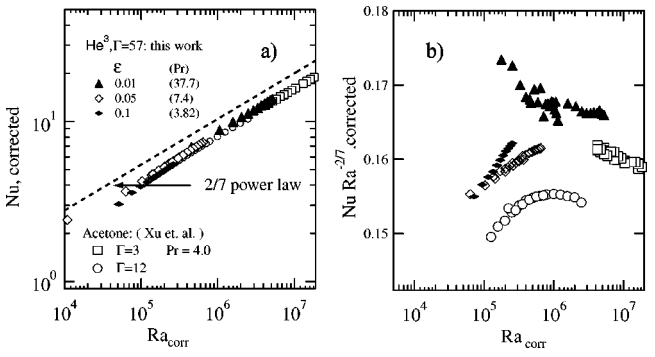

FIG. 7. (a) $\mathrm{Nu_{corr}}$ versus $\mathrm{Ra_{corr}}$ plot for various values of ϵ from this paper, and comparison with the data of Xu *et al.* obtained with acetone. The corresponding values of Pr are given in parentheses. Dashed line shows a 2/7 power law with an arbitrary amplitude. (b) Sensitive scaled representation showing deviations from the 2/7th power law for the sets of data shown in (a).

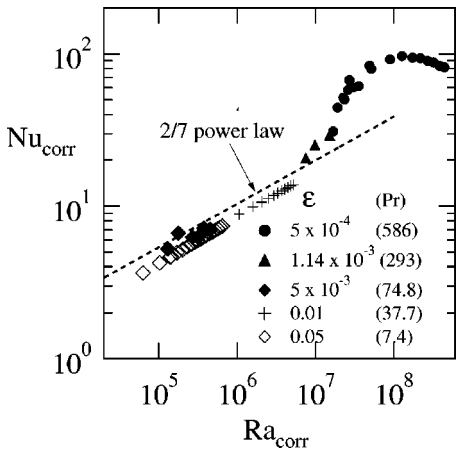

FIG. 8. $\mathrm{Nv_{corr}}$ versus $\mathrm{Ra_{corr}}$ at larger $\mathrm{Ra_{corr}}$ and highest Pr numbers. The dashed line again has an arbitrary amplitude.

Similarly to Ref. [21], we present in our Fig. 7(b) the more sensitive ratio $\mathrm{Nu_{corr}Ra_{corr}^{-2/7}}$ versus $\mathrm{Ra_{corr}}$, where the exponent (2/7) is a convenient representation of experimental data over a large range of Ra [22]. The very recent extension of the GL theory to Prandtl numbers over 12 decades up to 10^6 [46] will permit a comparison of our results with theory in the near future. We note in Fig. 7(b) the systematic change in the slope of the data curves as Pr is increased over a comparable range of $\mathrm{Ra_{corr}}$. The uncertainty in the parameters of ^{3}He at a given ϵ causes an uncertainty of the order of $\pm 5\%$ in the absolute value of Nu and Ra. As a result, the change of Nu with Pr at constant Ra for $10^5 < \mathrm{Ra} < 10^6$ cannot be estimated with precision, but it appears to be of the order of 10% or less.

While the data with Pr numbers below $\approx$50 show a smooth increase of Nu with Ra and follow the expected power law, those at the highest Pr numbers show a surprising and unexplained behavior. Figure 8 shows a rise of the data points for Pr=293 and 586 above this power law, followed by a maximum. In particular, the negative slope of Nu with increasing Ra is contrary to expectations. We note that a plot of the (corrected) convective current $(\mathrm{Nu}-1)\mathrm{Ra}$ versus Ra does not show the negative slope of the Nu(Ra) plot at the highest Ra numbers. We further note that the primary data are $\Delta T(q)$, which were obtained in four different series of experiments. These data used the same routine as those at lower values of Pr and where the fluid behavior appeared normal, and care was taken to stay within the Boussinesq criteria mentioned before. We are unclear whether at the largest compressibilities the ''ATG'' corrections, Eqs. (6) and (9), are still sufficient and appropriate for the calculation

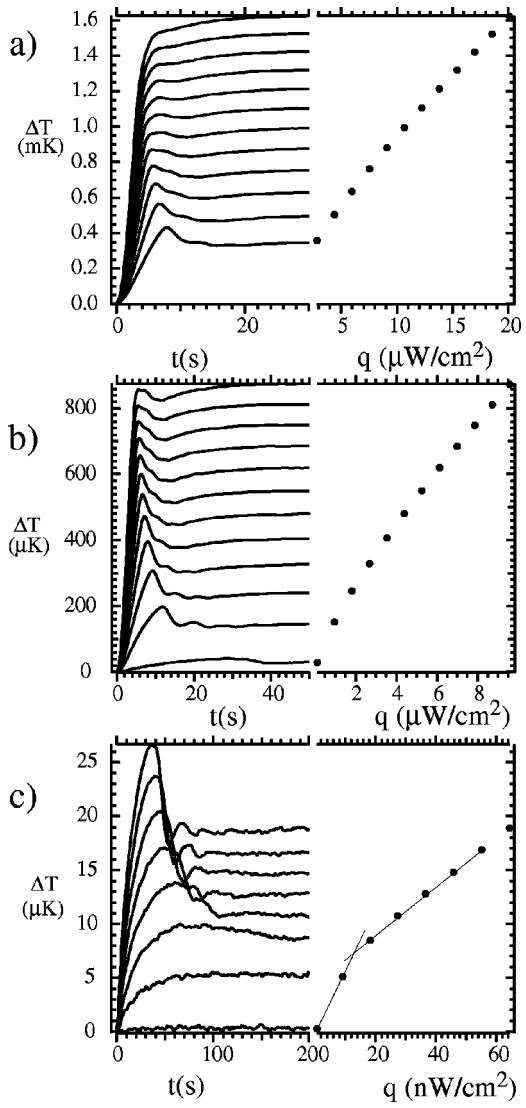

FIG. 9. Left side: selected transient profiles $\Delta T(t)$ at $\epsilon = 5 \times 10^{-2}$ for various heat currents q after ''heat-on.'' Right-hand side: the corresponding steady state $\Delta T(\infty)$ versus q. The figures (a), (b), and (c) with progressively higher q represent separate sets of experiments. The shape of a transient changes from a simple ''overshoot'' to damped oscillation, then to a simpler shape at still larger values of q.

of Nu(Ra). These results need to be verified with further experiments on ^{3}He and other fluids closer to the critical point with still higher values of Pr.

B. Transient data

We present our data in order of increasing values of q, and chose as a representative example a series of traces at an intermediate temperature $\epsilon = 5 \times 10^{-2}$. Figure 9(a), 9(b), and 9(c) show the evolution with q increasing from the bottom to top, for the most convenient representation. Figure 9(c) shows the evolution of $\Delta T(t)$ first in the diffusive regime and further as q increases above the onset of convection ($\Delta T > 7.5\,\mu$K). On the left side, the traces are obtained after starting the heat current q at $t = 0$ and where the steady state

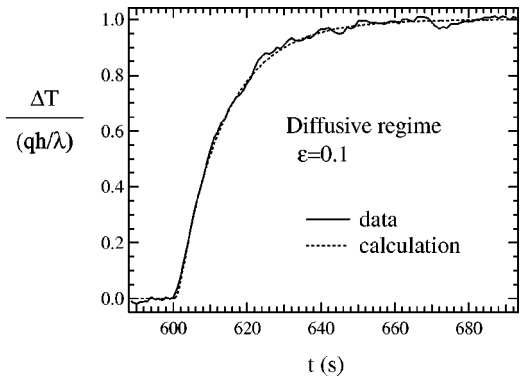

FIG. 10. $\Delta T(t)$ transient in the diffusive regime for $\epsilon = 0.1$ and $\Delta T(\infty) = 12.5\,\mu$K after turning the heat on at $t = 600$ s, shown by the noisy line. Solid curve: prediction as described in the text and in the Appendix, without free parameters.

$\Delta T(\infty)$ is reached within $\approx$200 s. The right-hand plot shows the steady state $\Delta T(\infty)$ versus q. The break in the curve for $\Delta T_{\text{onset}} = 7.5\,\mu$K reflects the onset of convection for higher values of q.

We now examine and analyze the results in the diffusive regime, and then for q beyond the onset of convection.

1. Diffusive regime

In Fig. 10 a normalized trace is presented for $q = 12$ nW/cm^2 at $\epsilon = 0.1$, for the ''heat-on'' process, where $\Delta T(\infty) = 12.0\,\mu$K, and stratification from gravity is negligible. The trace is compared with predictions [28] (solid line) without adjustable parameters. The calculations use the values of D_T and $\gamma \equiv C_P/C_V$ determined experimentally in this laboratory, and an outline of the theory is given in the Appendix. Generally, for a given ϵ, we find that the data at various values of q, when normalized to the corresponding value of $\Delta T(\infty)$, overlap within the scatter of the noise. This is particularly noteworthy for $\epsilon > 0.05$, where ΔT_{onset} becomes large, making it possible to generate traces in the diffusive regime over a wider range of q. This result implies that the diffusive relaxation time τ is independent of $\Delta T(\infty)$, as expected.

We note that since the experiment takes place at constant $\overline{\rho}$, reaching a steady state is therefore influenced by the adiabatic energy transfer (''Piston effect'') after turning the heat on or off [28]. This transient is given by a more complicated mathematical expression than the simple diffusive process observed at constant pressure. In the Appendix B we present a short discussion on the effect of the adiabatic energy transfer on the fluid stability after turning the heat flow on.

The diffusive relaxation time has been obtained by an exponential fit of the transient $|\Delta T(t) - \Delta T(\infty)|$ versus t both after turning the heat on and off; this is when the ''tail'' amplitude is less than $\approx$1/3 of the total steady-state span $\Delta T(\infty)$. As shown by Behringer *et al.* [30], the exponential fit $\exp(-t/\tau_0)$ gives the slowest mode relaxation time as

$$\tau_0 = \left(\frac{h}{A(\epsilon)}\right)^2 \frac{1}{D_T}, \tag{11}$$

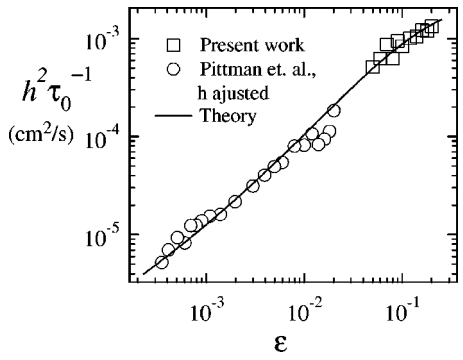

FIG. 11. Scaled relaxation rate $h^2\tau_0^{-1}$ versus ϵ. Open squares: present data, open circles: Pittman *et al.* with the height h increased by 8%, as described in text. Solid line: predictions, as described in the text.

where $A(\epsilon)$ is a function of γ and changes from $\pi/2$ to π as $\gamma(\epsilon)$ varies from 1 to ∞. This calculation explained the majority of the large discrepancy between the experimental relaxation times and those expected based on the measured conductivity values as reported by Pittman *et al.* [29] However, Behringer *et al.*'s analysis of Pittman's data showed that there was still a remaining discrepancy of the order of approximately 10%, which was not understood at the time.

The data for τ_0^{-1} obtained in this experiment, scaled by h^2, are plotted versus ϵ in Fig. 11. As discussed in the Appendix, our data suggests that in the earlier experiments [29] the value of the cell height h was determined incorrectly, which introduced approximately an 8% error in λ. We replotted the scaled relaxation times reported in Ref. [29] using the corrected value of h, and found that it eliminated all the discrepancies between these and the calculations of Behringer *et al.* Thus the experimental and expected relaxation times are in agreement, both for our most recent data and for those of Ref. [29], provided the cell height used in those experiments is corrected.

2. Convective regime: Data

For $\Delta T > \Delta T_{\rm onset} \approx 7.5\,\mu$K, Fig. 9(c) shows that a gradual ''overshoot'' emerges with increasing q, as observed in previous work with liquid ^{4}He at saturated vapor pressure [47,42,48]. By contrast, the overshoot decay in the present traces is not simply exponential but evolves into damped oscillations where both the damping and the oscillation rates increase with q. These seem to have not been reported previously. We also observe the critical slowing down of the convective relaxation rate $\tau_{\rm RB}^{-1}$ as the onset of convection is approached from the higher values of ra* as found by Behringer and Ahlers [47]. This is consistent with the expectations, as described by Behringer [48].

Figures 9(a) and 9(b) show the evolution of $\Delta T(t)$ at small times, well before the steady state has been reached, and where the traces were recorded over a period of 900 s. Some traces have been suppressed to avoid overcrowding the plot. Again the right-hand side shows $\Delta T(\infty)$ versus q. At still higher heat currents, the oscillation amplitude decreases, and the ''overshoot'' gradually disappears. When q is turned

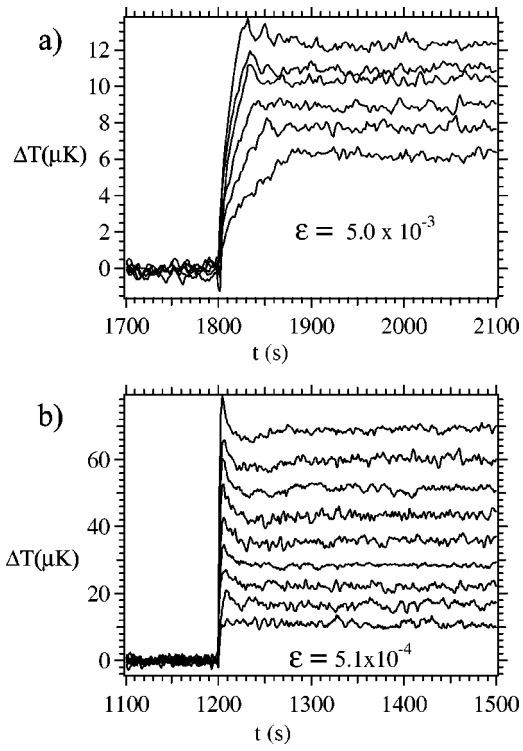

FIG. 12. $\Delta T(t)$ transient profiles for $\epsilon = 5\times10^{-3}$ and 5×10^{-4}, to be compared with those at $\epsilon = 0.05$ in Fig. 9(c). The $\Delta T_{\rm onset}$ is less than 4 μK for both sets of data. Note the absence of the overshoot and of the damped oscillations for the traces taken at comparable ΔT to Fig. 9(c) above the convection onset.

on, the initial rise of ΔT becomes more rapid as the fluid system is driven harder. Steady state is reached already after about 20 s for the highest values of q, compared with times of order 300 s in the regime below and just above the convection onset. The type of behavior shown here is representative for the traces at $1\times10^{-2} \leqslant \epsilon \leqslant 2\times10^{-1}$ investigated in these experiments.

As ϵ decreases below $\approx 9\times10^{-3}$, the damped oscillations are not observed as clearly. After the heat current has been turned on, the steady state in the convective regime immediately above the onset (this is for $\Delta T \geqslant 3.7\,\mu$K) is reached much faster than in the diffusive regime. An overshoot does not develop until well above the convection onset for $\Delta T(\infty) > 12\,\mu$K. This is shown in Figs. 12(a) and 12(b) for two representative examples at $\epsilon = 5\times10^{-3}$ and 5×10^{-4}, where the transient profile is to be contrasted to that in Fig. 9(c) at $\epsilon = 5\times10^{-2}$. After the heat flow has been turned off, there is correspondingly a strong difference in the decay of $\Delta T(t) \to 0$ between the traces at $\epsilon = 5\times10^{-2}$ and 5×10^{-4}. In the first case there is a smooth decrease to zero, while in the second one, the signal decays very rapidly to $\Delta T \approx 0$, rebounds, and is followed by a maximum before $\Delta T = 0$ is asymptotically reached.

A detailed summary of the domains corresponding to these different features in the $\Delta T(\infty) - \epsilon$ plane has been presented elsewhere [14]. We note that there seems to be a marked change in the transient pattern for $\epsilon < 9\times10^{-3}$, both after the heat current is turned on and also off. It will be

interesting to understand what factors are responsible for this change, whether the diverging Pr or the compressibility or both.

3. Convective regime: Transient experiments and simulations

Amiroudine *et al.* [49] have carried out a two-dimensional (2D) numerical simulation of the onset of instabilities in a near-critical fluid (CO_2) at the critical density in a RB configuration. In their system, a square cavity with $h = 10\,\mathrm{mm}$, the boundary conditions differ from those in our experiment as follows: In the simulation a temperature difference ΔT is established across the fluid within approximately 2 s, and where the heat flux is left floating. The local parameters ρ, T, and particle velocity v are then calculated at various times, showing the evolution of the bottom (hot) and top (cold) boundary layers with time and the formation of ''plumes'' in the convective state, both on the hot and on the cold layers. By contrast, in our laboratory experiment, the bottom temperature is left floating, and tends to a steady-state value some time after turning on the constant heat flow q.

Preliminary results have been reported by Amiroudine *et al.* [27] on their results of a 2D numerical simulation for ^{3}He near the critical point. This is done with identical parameters and boundary conditions as those in our laboratory experiment, and using a similar RB configuration with cell height $h = 1\,\mathrm{mm}$ and $D = 50\,\mathrm{mm}$. In a control simulation, very good agreement was obtained with our data in the diffusive regime at several values of ϵ. In the convective regime for $\epsilon = 0.01$, the simulation produced the expected ''overshoot'' both in magnitude and in time scale agreement with the laboratory experiment.

4. The noise spectrum

Examination of individual (not signal-averaged) traces of ΔT (steady state) as a function of t shows no convincing evidence of periodic oscillations, fluctuations or bursts, such as reported in previous experiments reviewed by Behringer [48]. Even for $\mathrm{Ra}_{\mathrm{corr}} \gg 1708$, the noise in the traces is only twice that for $q = 0$. We have calculated the power spectrum of $\Delta T(t)$ in the steady state. The results for the highest power with $\mathrm{Ra}_{\mathrm{corr}}/\mathrm{Ra}_c = 132$ at $\epsilon = 0.1$ were compared with the spectrum for zero heat, in a form identical to that in Behringer's work for ^{4}He at saturated vapor pressure (Fig. 22 in Ref. [48]). Although we do observe the increase in fluctuations with q, a substantially higher relative noise level in our experiments prevents a systematic study of the fluctuation spectra at various reduced temperatures near T_c. From our present data, there is no clear signature for the onset of turbulence, in contrast of what was observed with liquid ^{4}He. For details, we refer to Ref. [14].

V. CONCLUSION

We have presented the steady-state results for the temperature difference $\Delta T(t)$ across a fluid layer along the critical isochore for ^{3}He obtained in a Rayleigh-Bénard cell with an aspect ratio of $\Gamma = D/h = 57$. The first part of this program consists in the systematic study of the steady-state onset of convection as the ATG criterion becomes dominant when the compressibility diverges as the critical point is approached. In the second part, we have investigated the transients, both in the diffusive and in the convective regimes, after turning the heat flow on (and off), until steady state was reached. Our results are as follows:

(1) We have observed the crossover of the convection onset condition from the classic Rayleigh regime, where dissipative effects determine the transition to convection, to the regime dominated by the ATG or ''Schwarzschild'' criterion. Close to T_c, when $C_p \gg C_v$, the nonzero ATG stabilizes the fluid against convection as long as the fluid density decreases in the upward direction. The transition curve $\Delta T_{\mathrm{onset}}(\epsilon)$ obtained experimentally in the steady state is in very good agreement with predictions.

(2) In the convective regime, the correction for the ATG effect through introducing the potential temperature θ collapses the plots of the convective current vs reduced Rayleigh number onto a common line. The value of the initial slope of the scaled data, obtained above the convection onset, agrees with the experiments on other fluids in RB cells with a similar aspect ratio and with a much smaller compressibility than supercritical ^{3}He. The numerical value of the slope is closest to the calculated one for a flow pattern given by a family of straight parallel rolls, and disagrees with the calculations for a concentric rolls pattern found most commonly with fluids.

(3) The experiments in the early turbulent convective regime with Rayleigh numbers up to 5×10^8 have been presented, together with comparison with other data at similar Pr. The Nu versus Ra presentation (with both numbers corrected for the ATG effect) for $\mathrm{Pr} < 40$ is compared with high-precision data on acetone with $\mathrm{Pr} = 4$ [21]. A surprising and unexplained behavior is shown for the two highest Pr numbers (293 and 586) indicating a significant departure from the expected power-law behavior.

The transient $\Delta T(t)$ results are as follows:

(4) In the regime without convection, the experimentally obtained curves agreed with predictions. Our combined measurements of the thermal conductivity and the diffusive relaxation time allowed to identify the source of the discrepancy between these quantities reported in the earlier experiments and justified a simple correction to earlier data, as proposed in the Appendix.

(5) In the convective regime, the previously reported overshoot in ΔT after turning on the heat has been observed, but it was followed by an unusual pattern of damped oscillations before a steady-state was reached. The gradual evolution of the temperature transient with further increasing q has been described. Computer simulations by Amiroudine *et al.* presently in progress, can help clarifying these observations.

ACKNOWLEDGMENTS

The authors are indebted to D. Murphy, who participated in the design of the RB cell and in initial data taking, for many discussions and good advice. We have benefited from

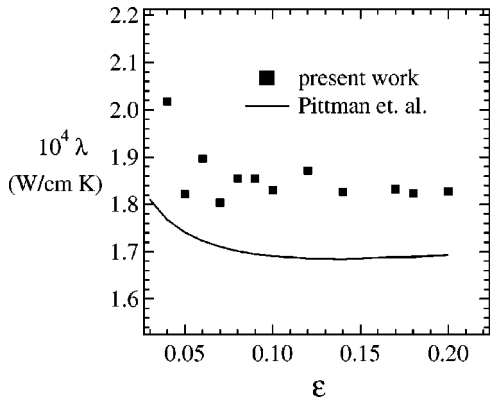

FIG. 13. Thermal conductivity of ^{3}He along the critical isochore. Solid circles: present data. Solid line: fit to the conductivity data obtained by Pittman *et al.*

stimulating discussions and continued interaction with S. Amiroudine and P. Bontoux and from correspondence with V. Steinberg, F. Busse, and D. Lohse. We also acknowledge informative discussions with B. Castaing, R. P. Behringer, H. S. Greenside, and G. Ahlers. Comments and suggestions on this manuscript by D. Goodstein and S. Amiroudine and the gift of a Ph.D. thesis copy by X. Chavanne have been greatly appreciated. This research has been supported by NASA Grant No. NAG3-1838.

APPENDIX

1. Thermal conductivity

Measurements of the thermal conductivity λ with the heat flowing upwards were made in the diffusive regime at the same temperatures as the convection measurements. The data extend to higher values of ϵ those of Pittman *et al.* [29] and by Cohen *et al.* [50], obtained with a regular conductivity cell where the heat flows downwards, therefore stabilizing the fluid. The accuracy of our present measurements, with heat flowing upwards, was limited by the allotted range of ΔT in the diffusive regime, and it degraded for $\epsilon < 0.05$, with the maximum $\Delta T \approx 3.5\,\mu$K, the value fixed by the ATG criterion. The new data and those of Ref. [29] are presented in Fig. 13. A systematic discrepancy of $\approx$8% between the sets of measurements above $\epsilon = 0.05$ is found. (The data by Cohen *et al.*, taken in a more complicated thermal conductivity cell with an uncertainty in the effective value of h, have not been included.) For $\epsilon < 0.05$, the rapid increase of the apparent λ observed in the present paper reflects the rounding of the transition due to partial convection in the cell, and these data will not be considered further.

We believe that the origin of the discrepancy lies in the incorrect determination of h in the cell of Ref. [29] with $h = 0.032$ cm, compared to our convection cell with $h = 0.106$ cm. We checked this assumption by comparing the observed relaxation times with the expectations based on the measured λ and thermodynamic properties of the fluid (see Fig. 11). We found that the discrepancy between the observed and expected relaxation times reported in Refs. [30, 51] is eliminated when the cell height used in Ref. [29] was taken to be $h = 0.032 \times 1.08 = 0.0345$ cm. This adjustment, which increases D_T by 8%, also leads to an improved agreement within the combined uncertainties between the measured and the calculated linewidth of scattered light for ^{3}He near the critical point (Fig. 5 in Ref. [52]).

2. Impact of the Piston effect

The term ''piston effect'' describes the mechanism of adiabatic temperature relaxation, which emerges in compressible fluids under fixed total volume conditions, and qualitatively changes the equilibration scenario as compared to ordinary heat diffusion. There are distinct ways in which the piston effect is expected to affect our measurements:

(1) During the transient, even before the fluid starts convecting, the presence of the piston effect modifies the temperature and density spatial distribution compared to an ordinary diffusive relaxation process. A proper analysis of the relaxation with the piston effect presence allows to identify which regions inside the layer are the most unstable during the transient, and is therefore important for understanding our $\Delta T(t)$ results. This will be treated in detail later in this section. A complete analytical treatment can be made for a fluid where the properties can be assumed to be independent of temperature and density variations within the layer.

(2). The fluid flow in the convective regime is likely to be affected by the piston effect, and this has been discussed in the work of Amiroudine *et al.* [49]. The density of a given fluid element may be changing substantially during its travel across the cell compared to the Boussinesq case. Such variations in density will couple with the corresponding fluid temperature in the cell through the piston effect, and this coupling might produce unexpected results. In our opinion, this is an interesting and still open question. We hope that computer simulations by Amiroudine and co-workers [26] will provide clues regarding the role of the piston effect during convection.

Below, we present calculations of the temperature response to an external disturbance under conditions when the piston effect is non-negligible. The response of a compressible fluid at fixed average density (fixed total volume) is sensitive to the choice of the boundary conditions, or, equivalently, to the form of the disturbance. Below we consider the two scenarios A and B to obtain the steady-state data in our cell. Both assume that the top plate is always kept at constant temperature during the measurement, and the fluid is initially in equilibrium.

Case A: The measurement is initiated by forcing the temperature of the bottom plate, $T_{\rm bot}$, to increase rapidly by some finite ΔT, which then equals the temperature difference $\Delta T(t=\infty)$ across the fluid. This will initially produce thin layers of denser fluid at the top and lighter fluid at the bottom of the cell, a typical signature of the piston effect. In the paper by Amiroudine *et al.* [49], the point is made that the small initial width of the boundary layer has a higher convection onset ΔT than the bulk fluid, and therefore stabilizes the fluid. With increase of time, where the width of both boundary layers increase, the fluid stability decreases, but then increases again under the effect of the ATG. We em-

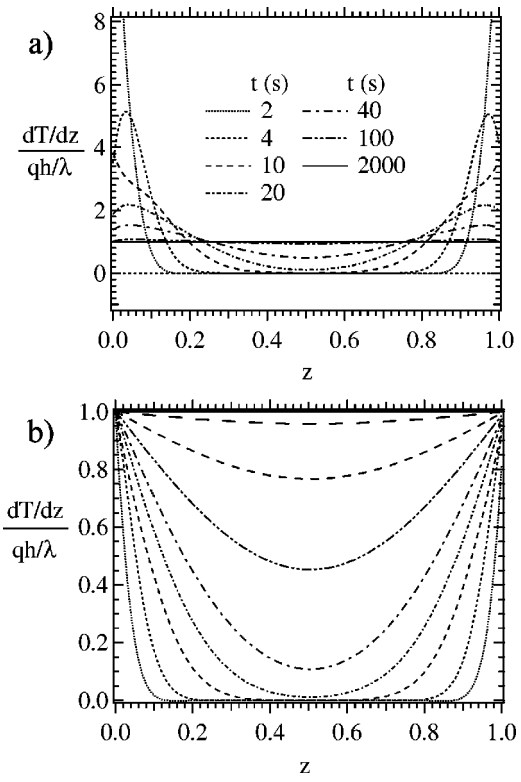

FIG. 14. The normalized local vertical temperature gradient across the layer versus time t and vertical location $z=x/h$ for two different boundary conditions at the bottom surface, both starting with the cell initially in a thermal equilibrium at $\epsilon=0.01$. (a) Bottom temperature raised stepwise by fixed amount, and q floating. (b) Bottom plate temperature floating, and q is turned on in a stepwise manner.

phasize that this would only affect the transient, and would be irrelevant for steady-state measurements.

Case B, which corresponds to our experimental conditions: The temperature $T_{\rm bot}$ is left floating, the heat flux (q = const.) is turned on, and the bottom plate is allowed to reach the final (steady-state) temperature. Numerical calculations of the density profile for this boundary condition at the bottom [Ref. [51], Fig. 7(a)] showed that unlike in Case A, the density gradient at both boundary layers at short times after heat is turned on, never exceed the final value at any point of the cell. No boundary layers of large, rapidly changing temperature or density gradients are produced. This means that if the final temperature difference is smaller than $\Delta T_{\rm onset}$, the fluid is always stable throughout the measurement. Therefore in our experiments in the nonconvective state, the piston effect does not play a significant role in the stability of the fluid.

In Fig. 14 we present a plot of the local vertical temperature gradient as a function of vertical location z at various times t, computed at $\epsilon=0.05$: (a) case A where the temperature of the bottom plate is suddenly raised by $\Delta T(\infty)$ and q is floating, (b) case B for fixed q and floating bottom plate temperature until it reaches $\Delta T(\infty)$. These plots have been computed in a similar way as described in Ref. [13]. In the first case, very large temperature gradients are generated at the boundaries immediately after the bottom temperature is stepped up. By contrast, in case B, the temperature gradient never exceeds the final value anywhere in the cell during the transient. The almost flat curve with long dashes reflects conditions close to steady state.

3. Transient in the diffusive regime

As will be shown below, the transient $\Delta T(t)$ in this regime, predicted by the Onuki–Ferrell theory [28] can be calculated analytically and compared with the experimentally measured $\Delta T(t)$. This comparison was made to verify that the apparatus is functioning properly. The method is the same as that already described in Ref. [53], but with boundary conditions adapted to a thermal conductivity cell. Here we briefly outline the method, and refer to Ref. [14] for the detailed derivation.

When the fluid is kept at constant average density, the equation for the temperature inside the cell in the linearized Onuki-Ferrell approximation reads

$$\frac{\partial T}{\partial t}=\alpha\frac{\partial [T]}{\partial t}+D_T\frac{\partial^2 T}{\partial x^2}, \tag{A1}$$

where [...] means averaging over space. Here x is the vertical coordinate and $\alpha\equiv(1-\gamma^{-1})$. This equation can be solved in a way similar to that described in Ref. [53]. We only outline this method here with the boundary conditions appropriate to a conductivity cell, which are

$$q(t)=0, \quad t<0, \tag{A2}$$

$$q(t)=q_0, \quad t>0, \tag{A3}$$

$$T(xt)_{x=h}=T_{\rm top}. \tag{A4}$$

Here the heat flux q_0 is applied to the bottom plate. In the frequency (ω) space, one defines a complex response function $Z(\omega,x/h)$ by

$$Z(\omega,z)=\delta T^*(\omega,z)/\Delta T(q_0), \tag{A5}$$

where $\delta T^*(\omega,x/h)$ are the Fourier components of the temperature difference $\delta T(t,x/h)=[T(t,x/h)-T_{\rm top}]$ and $\Delta T(q_0)=q_0 h/\lambda$ is the steady-state value of δT at $x=h$. Upon Fourier transforming Eq. (A1) and applying the boundary conditions, the function $Z(\omega,z)$ is obtained. In order to obtain the response $\Delta T(t)$ in real time, a direct and inverse Fourier transform operation is used, as given in Refs. [13] and [14].

An alternative approach was used in Ref. [51]. In that work, the solution of Eq. (A1) was developed in the form of a series directly in time-space coordinates. Both methods give the same results, however the use of the response functions in frequency space is slightly more flexible for the following reasons: First, the same expression in frequency space allows to calculate the response to an arbitrary time-dependent flux $q(t)$, should such conditions be used in future experiments or in numerical simulations. Second, as discussed below, the response function method allows making corrections for instrumental time scales in a simple fashion.

In Fig. 10, Sec. IV B 1, we have shown the comparison between the observed transient and the analytical solution at $\epsilon=0.1$, and noted the good agrement. Here the analytical response function used in the calculation was corrected for the presence of a double-pole low-pass filter at the output of the phase-sensitive amplifier used for the $\Delta T(t)$ measurements. To perform such an adjustment, the solution for $Z(\omega,z)$ given by Eq. (A5) needs to be multiplied by the filter response function

$$L=\frac{1}{(1+i\omega\tau_F)^2}. \tag{A6}$$

The time constant of the filter was $\tau_F=1.25\,\mathrm{s}$ and is responsible for the noticeable ''lag'' during the first seconds of the relaxation, visible both in the calculated curve and in the experimental trace. No corrections for either heat capacity of the bottom plate or conductivity of the sidewall were made, because a previous analysis of their contributions [30] showed them to change the fluid relaxation time τ in a negligible way.

4. Transport properties along the critical isochore

The C_p values, based on compressibility and density data, were calculated using the common thermodynamic relation with C_v, where the data [54] had again to be extrapolated beyond $\epsilon=0.05$. The good internal consistency for D_T obtained from the relaxation times, from the ratio λ/C_p, and also implied by the light scattering experiments [52] indicated that the extrapolation was adequate. The values of λ used for the calculations of D_T are obtained from by increasing the values of Pittmann by 8%.

A tabulation of static and transport properties used in the convection work with the ajusted value of λ is available on request as a postscript document.

[1] D. J. Tritton, Physical Fluid Dynamics (Oxford Science, Oxford, 1988), Section 14.6 and Appendix.

[2] A. Schlueter, D. Lortz, and F. Busse, J. Fluid Mech. **23**, 129 (1965).

[3] G. Ahlers, M. Cross, P. Hohenberg, and S. Safran, J. Fluid Mech. **110**, 297 (1982).

[4] S. Gauthier, T. Desmarais, and G. Iooss, Europhys. Lett. **10**, 543 (1989).

[5] E. A. Spiegel, Annu. Rev. Astron. Astrophys. **9**, 323 (1971).

[6] X. Chavanne *et al.*, Proceedings LT21, Czech. J. Phys. **46** (Suppl S1), 91 (1996).

[7] Sh. Ashkenazi and V. Steinberg, Phys. Rev. Lett. **83**, 3641 (1999).

[8] L. D. Landau and E. M. Lifshitz, *Course of Theoretical Physics: Vol. 6 Fluid Mechanics* (Pergamon, Oxford, 1959).

[9] M. Gitterman and V. Steinberg, Vys. Temp. **8**, 799 (1970) [High Temp. USSR **8**, 754 (1970)].

[10] M. Gitterman and V. Steinberg, Prikl Mat. Mekh. **34**, 325 (1970) [J. Appl. Math. Mech. USSR **34**, 305 (1971)].

[11] M. Gitterman, Rev. Mod. Phys. **50**, 85 (1978).

[12] P. Carlès and B. Ugurtas, Physica D **126**, 69 (1999).

[13] A. B. Kogan and H. Meyer, J. Low Temp. Phys. **112**, 419 (1998). Here the listing of $T_c=3.3190\,\mathrm{K}$ was accidentally omitted, but has been presented in the Ph.D. thesis by A. B. Kogan.

[14] A. B. Kogan, Ph.D. thesis, Duke University, 2000 (unpublished), available as a pdf document.

[15] F. Zhong and H. Meyer, Phys. Rev. E **51**, 3223 (1995).

[16] M. Assenheimer and V. Steinberg, Phys. Rev. Lett. **70**, 3888 (1993).

[17] Sh. Ashkenazi, Ph.D. thesis, Weizmann Institute of Science, Rehovot, Israel, 1997 (unpublished).

[18] X. Chavanne *et al.*, Phys. Rev. Lett. **79**, 3648 (1997).

[19] X. Chavanne, Ph.D. thesis, Université Joseph Fourier, Grenoble, Oct. 1997 (unpublished).

[20] J. J. Niemela, L. Skrbek, K. R. Sreenivasan, and R. J. Donnelly, Nature (London) **404**, 837 (2000).

[21] X. Xu, K. M. S. Bajaj, and G. Ahlers, Phys. Rev. Lett. **84**, 4357 (2000).

[22] S. Grossmann and D. Lohse, J. Fluid Mech. **407**, 27 (2000).

[23] A. Kogan, D. Murphy, and H. Meyer, in NASA Document D-18925, 2000, p. 197.

[24] A. Kogan, D. Murphy, and H. Meyer, Phys. Rev. Lett. **82**, 4635 (1999).

[25] A. Kogan, D. Murphy, and H. Meyer, Physica B **284**, 208 (2000).

[26] S. Amiroudine, P. Bontoux, and B. Zappoli (private communication, 1999).

[27] S. Amiroudine, A. B. Kogan, H. Meyer, and B. Zappoli, Proceedings of the 20th International Congress of Theoretical and Applied Mechanics, ICTAM 2000, Chicago, edited by J. W. Phillips (unpublished).

[28] A. Onuki and R. A. Ferrell, Physica A **164**, 245 (1990).

[29] C. Pittman, L. H. Cohen, and H. Meyer, J. Low Temp. Phys. **46**, 155 (1982).

[30] R. P. Behringer, A. Onuki, and H. Meyer, J. Low Temp. Phys. **81**, 71 (1990).

[31] In the paper by Carlès and Ugurtas [12], Fig. 2 shows the predicted vertical gradient $\partial\Delta T_{\mathrm{onset}}/\partial z$ for CO_2 as a function of $T-T_c$ for various values of h, and illustrates how the shape of the convection onset curve changes with h. For $h>5$ mm, the Rayleigh regime is no longer observable for $T-T_c>20\,\mathrm{K}$, this is for $\epsilon>0.07$. These plots are very similar to those for ^{3}He we have produced during the design stage of our experiment.

[32] C. C. Agosta, S. Wang, L. H. Cohen, and H. Meyer, J. Low Temp. Phys. **67**, 237 (1987).

[33] S. Wang, C. Howald, and H. Meyer, J. Low Temp. Phys. **79**, 151 (1990).

[34] C. Pittman, T. Doiron, and H. Meyer, Phys. Rev. B **20**, 3678 (1979).

[35] D. Murphy, J. Low Temp. Phys. **114**, 389 (1999).

[36] G. Ahlers has pointed out that in convective turbulence, where the temperature profile through the fluid layer is stronly non-

linear, the assumption of parallel heat flow though the walls and the fluid is not correct. However his numerical simulations using the thermal conductivity of ^{3}He, the aspect ratio of the cell and the conductance of the stainless steel wall indicate that for our high aspect ratio, the assumption mentioned above appears to introduce only a negligible error. We are very much obliged to Ahlers for attracting our attention to this point and for his calculation.

[37] J. M. Pfotenhauer and R. J. Donnelly, Adv. Heat Transfer **17**, 65 (1985).

[38] J. S. Olafsen and R. P. Behringer, J. Low Temp. Phys. **106**, 673 (1997).

[39] J. A. Lipa and Q. Li, Proceedings LT21, Czech. J. Phys. **46** (Suppl S1), 185 (1996).

[40] A. Patashinski and A. Burin, NASA Document No. D-18925, 2000, p. 301.

[41] D. Murphy and H. Meyer, J. Low Temp. Phys. **97**, 509 (1994).

[42] R. Behringer and G. Ahlers, J. Fluid Mech. **125**, 219 (1982).

[43] C. W. Meyer, G. Ahlers, and D. Cannell, Phys. Rev. A **44**, 2514 (1991).

[44] A. L. Woodcraft, P. G. J. Lucas, R. G. Matley, and W. Y. T. Wong, J. Low Temp. Phys. **114**, 109 (1999).

[45] V. Croquette, Contemp. Phys. **30**, 153 (1989).

[46] S. Grossmann and D. Lohse, Phys. Rev. Lett. **86**, 3316 (2001).

[47] R. P. Behringer and G. Ahlers, Phys. Lett. A **62**, 329 (1977).

[48] R. Behringer, Rev. Mod. Phys. **57**, 657 (1985).

[49] S. Amiroudine, P. Bontoux, P. Larroude, B. Gilly, and B. Zappoli, J. Fluid Mech. (to be published).

[50] L. H. Cohen, M. Dingus, and H. Meyer, J. Low Temp. Phys. **61**, 79 (1985).

[51] F. Zhong and H. Meyer, J. Low Temp. Phys. **114**, 231 (1999).

[52] Y.-I. Miura, H. Meyer, and A. Ikushima, J. Low Temp. Phys. **55**, 247 (1984).

[53] F. Zhong, A. B. Kogan, and H. Meyer, J. Low Temp. Phys. **108**, 161 (1997).

[54] G. R. Brown and H. Meyer, Phys. Rev. A **6**, 364 (1972).